

# Air-jet spun tissue engineering scaffolds incorporated with diamond nanosheets with improved mechanical strength and biocompatibility

Robin Augustine<sup>a,b,\*</sup>, Sumama Nuthana Kalva<sup>a,b</sup>, Yogesh B. Dalvi<sup>c</sup>, Ruby Varghese<sup>c,d</sup>, Maneesh Chandran<sup>e</sup>, Anwarul Hasan<sup>a,b,\*</sup>

<sup>a</sup> Department of Mechanical and Industrial Engineering, College of Engineering, Qatar University, P.O. Box 2713, Doha, Qatar

<sup>b</sup> Biomedical Research Center (BRC), Qatar University, P.O. Box 2713, Doha, Qatar

<sup>c</sup> Pushpagiri Research Centre, Pushpagiri Institute of Medical Science & Research, Tiruvalla, Kerala 689101, India

<sup>d</sup> Department of Chemistry, School of Sciences, Jain Deemed to be University Bangalore, Karnataka 560069, India

<sup>e</sup> Department of Physics, National Institute of Technology Calicut, Kerala 673601, India

## ARTICLE INFO

### Keywords:

Tissue engineering  
Polycaprolactone  
Nanodiamond  
Air-jet spinning

## ABSTRACT

The development of highly porous cell supportive polymeric scaffolds with sufficient mechanical strength has always been a challenging task in tissue engineering. The widely used nanofiber fabrication methods like electrospinning are time consuming and the obtained nanofibrous scaffolds are generally consist of compactly packed fibers, which affect proper cell penetration. On the other hand, air-jet spinning is an upcoming, less explored alternative approach for generating loosely arranged nanofibrous scaffolds within short time. However, air-jet spun scaffolds show inferior mechanical properties due to loosely organized fibers. Herein, we report the fabrication and detailed characterization of polycaprolactone (PCL) tissue engineering scaffolds loaded with diamond nanosheets (DNS) by air-jet spinning. Our results showed that the inclusion of DNS could improve the mechanical strength of the scaffolds. *In vitro* biocompatibility, and *in vivo* implantation studies demonstrated that PCL-DNS scaffolds are highly biocompatible and are suitable for tissue engineering applications. Our studies showed that mammalian cells can proliferate well in the presence of PCL-DNS scaffolds and the nanocomposite scaffolds implanted in rats did not show any considerable adverse effects. Overall, the findings show that the developed novel air-jet spun PCL-DNS nanocomposite scaffolds can be used as cell supportive scaffolds for various tissue engineering applications.

## 1. Introduction

Developing highly porous biodegradable scaffolds based on biodegradable polymers with desirable mechanical strength is one of the major steps in tissue engineering [1,2]. Such scaffolds can act as a support material for the adhesion, proliferation, and migration of cells to form tissues [3–5]. Air-jet spinning is a recently developed technique that can rapidly generate porous polymeric scaffolds composed of sub-micron fibers [6,7]. Air-jet spun scaffolds are highly promising for tissue engineering applications mainly because of their simple setup and fast processing, when compared to electrospinning technique- a well-established fibrous scaffold fabrication method [8,9]. These nanofibrous scaffolds have been shown to promote cell adhesion, migration, and angiogenesis [10–12]. Furthermore, their extracellular matrix (ECM)-like architecture, adjustable mechanical properties, and high

surface-to-volume ratio, which allows efficient cell attachment, making them a promising candidate for tissue engineering applications [13]. Polycaprolactone (PCL) is a biodegradable, biocompatible polymer with good mechanical properties and spinnability [14]. Nanofibrous scaffolds based on electrospun PCL are extensively investigated for various tissue engineering applications [15–19].

It is well known that a scaffold with poor mechanical strength will not function properly *in vivo* owing to the mechanical incompatibility with the surrounding tissue. Unfortunately, air-jet spun scaffolds show comparatively weak mechanical properties due to loosely arranged fibers. Recently, several nanomaterials such as zinc oxide (ZnO) [20,21], cerium oxide (CeO<sub>2</sub>) [22–25], and europium hydroxide (EHNs) [26] nanoparticles have been incorporated into scaffolds to improve their tensile strength. Two-dimensional (2D) nanomaterials, such as clays (nanosilicates) [27], bioglass nanostructures [28], hexagonal boron

\* Corresponding authors at: Department of Mechanical and Industrial Engineering, College of Engineering, Qatar University, P.O. Box 2713, Doha, Qatar.

E-mail addresses: [robin@robinlab.in](mailto:robin@robinlab.in) (R. Augustine), [ahasan@qu.edu.qa](mailto:ahasan@qu.edu.qa) (A. Hasan).

<https://doi.org/10.1016/j.colsurfb.2022.112958>

Received 28 August 2022; Received in revised form 6 October 2022; Accepted 19 October 2022

Available online 22 October 2022

0927-7765/© 2022 The Authors. Published by Elsevier B.V. This is an open access article under the CC BY license (<http://creativecommons.org/licenses/by/4.0/>).

nitride [29], carbon nitride, and layered double hydroxides [30], have been used for biomedical applications. Recently, carbon derivatives, such as carbon dots [31,32], carbon nanotubes [33], graphene, and its oxide [34], are utilized for tissue engineering applications. Nevertheless, these nanomaterials may suffer from biological incompatibility at higher loading, which is potentially detrimental to human health [35,36]. Therefore, finding highly safe nanofillers based on relatively inert material for improving the mechanical strength of tissue engineering scaffolds is highly demanding [37]. Recent reports indicate that diamond nanostructures with exceptional strength [38] and biocompatibility [39] can be used as nanofillers in tissue engineering scaffolds. Earlier studies showed that nanocrystalline diamond substrates can support cell adhesion, proliferation, and osteogenic differentiation of mammalian osteoblast-like cells [40–44] and osteoblasts [45,46]. Casted or molded poly(L-lactic acid) (PLLA)/nanodiamond scaffolds showed superior mechanical properties and similar cytocompatibility with that of neat PLLA [47,48]. Nanodiamond-loaded chitosan scaffolds also showed superior mechanical properties [49]. Some of the studies also indicated that polymeric nanofibrous scaffolds reinforced with nanodiamond particles can favor osteoblast proliferation [50].

In this paper, we report the fabrication of novel diamond nanosheets (DNS) impregnated PCL tissue engineering scaffold by air-jet spinning technique. Despite the appealing benefits and advancements in the preparation of various PCL composite nanofibres, the inclusion of diamond nanosheets as nano reinforcement in PCL-based composite nanofibres for tissue engineering has not been reported so far, to the best of our knowledge. Hence, in this study, we fabricated PCL-DNS composite scaffolds by air-jet spinning. Structure, morphology, and physicochemical properties of the developed scaffolds are characterized using X-ray Diffraction (XRD), scanning electron microscopy (SEM), high resolution transmission electron microscopy (HRTEM), and Fourier transform infrared (FTIR) spectroscopy, and differential scanning calorimetry (DSC). The biological performance of scaffolds is investigated by various *in vitro* and *in vivo* studies.

## 2. Materials and methods

### 2.1. Materials and reagents used

Polycaprolactone (PCL, Mw: 80,000), paraformaldehyde and (3-(4,5-dimethylthiazol-2-yl)-2,5-diphenyltetrazolium bromide) (MTT) were obtained from Sigma-Aldrich (USA). Dulbecco's Modified Eagle's Medium (DMEM) (Gibco) containing 10 % foetal bovine serum (FBS, Gibco) and 1 % penicillin-streptomycin solution (Gibco) was used for culturing cells. Live/Dead cell staining kit (Cat. No. R37601, Molecular Probes, Invitrogen, USA) was used for imaging live and dead cells. Nano/micro diamond particles were obtained from DeBeers (UK). All other reagents used in this study were from standard manufacturers and of analytical grade quality.

### 2.2. Preparation and characterization of DNS

As purchased diamond particles (500 mg) were dispersed in acetone (50 mL) and ultrasonicated (23 kHz) using an ultrasonicator (BioLogics-Inc, US) for 60 min to separate aggregated nanodiamond layers. Sonicated suspension was centrifuged at 1000 RPM to separate out larger diamond particles. Then, DNS were separated from the suspension by centrifuging at higher speed (10,000 RPM) and dried in a hot air oven (50 °C). The dried DNS were characterized by FTIR spectroscopy with Perkin Elmer Frontier MIR with PIKE Gladi ATR (USA) attachment and DTGS detector on a diamond crystal between 500 and 4000  $\text{cm}^{-1}$ . XRD patterns of DNS were recorded in the  $2\theta$  range of 10–90° using a Mini-Flex X-ray diffractometer using Cu K $\alpha$  radiation ( $\lambda = 1.5418 \text{ \AA}$ ) to characterize the crystallographic structure of the DNS. HR-TEM analysis was performed to examine the morphology, particle size, crystalline size of the DNS (JEOL JEM 2100). The crystallinity of the DNS and the

presence of crystallographic planes were determined using selected area electron diffraction (SAED).

### 2.3. Fabrication of PCL-DNS scaffolds

We used air-jet spinning method for the fabrication of bare PCL and PCL-DNS nanocomposites scaffolds. Air-jet spinning instrument consisted of an air compressor (La Padana 91016), an air brush (Master Airbrush) and a collecting board. The collecting board was covered with an aluminium sheet (30 cm  $\times$  30 cm size). PCL solutions with different concentrations of DNS were prepared in chloroform (10 mL). DNS were accurately measured and ultrasonicated for 15 min before PCL being added to chloroform to achieve maximum dispersion in the solvent. Then, to obtain a final concentration of PCL of 10 % w/v, a known quantity of PCL in pellet form was added to the above dispersions, and the mixture was magnetically stirred for 12 h until the pellet was fully dissolved. The prepared solutions were taken in air brush and spun over a collector by applying 80-psi air pressure. A 25 cm distance was maintained between the spray nozzle and the collector. It took 15–20 min to complete the fabrication. After completion of the process, the fibrous scaffolds deposited on the collector were carefully peeled out and stored in airtight polyethylene bags. For convenience, the scaffolds containing 0.5 %, 1 %, 2 % and 4 % (w/w) of DNS are denoted henceforth as PCL-DNS-0.5, PCL-DNS-1, PCL-DNS-2 and PCL-DNS-4, respectively. Air-jet spun PCL scaffolds without any DNS are designated as PCL.

### 2.4. Physicochemical characterization of PCL and PCL-DNS scaffolds

The morphological characteristics of prepared scaffolds were studied using SEM (FEI Nova-NanoSEM, 450) at 10 kV acceleration voltage. Samples were sputter coated with gold for 15 s, prior to the SEM analysis to improve the conductivity of the sample surface. Individual fibre diameter was calculated from SEM images using ImageJ software, and the average value was calculated from at least 100 fibres.

Interaction between the DNS and PCL as well as vibrational characteristics of nanocomposites were examined by FTIR analysis (Ref. Section 2.2 for the details). Crystallinity and the presence of nanosheets in PCL nanocomposite scaffolds is detected by XRD analysis (Ref. Section 2.2 for the details). Mechanical characteristics of nanocomposites is determined using a universal testing machine (Tinus Olsen H50 KT Universal Testing Machine, USA) according to the ASTM D 882 standard by applying a 500 N load cell at a crosshead speed of 1 mm  $\text{min}^{-1}$ . In each case, 5 samples were tested. All the samples had dimensions of 6 cm  $\times$  1 cm.

### 2.5. *In vitro* cell culture studies

The cytocompatibility of scaffolds was tested using human keratinocyte cells (HaCaT cells, Passage-26) and mouse fibroblasts (3T3 cells, ATCC CRL-1658, Passage-34). Cells were grown at 37 °C with 5 %  $\text{CO}_2$  supply in Dulbecco's modified Eagle's medium (DMEM) containing 10 % foetal bovine serum and 1 % streptomycin – penicillin solution. Samples were cut into discs with 8 mm diameter using paper punches, then, sterilized by dipping in 70 % alcohol (10 min) and ultraviolet treatment (for 15 min). Sterilized samples were placed in the wells of 96 well plates, which were pre-seeded with cells at 25,000 cells per sample on each scaffold and cultured for different time points (24 h, 5-days) in appropriate media as described above. To visualize the proliferation of cells in the presence of scaffolds, live/dead staining was performed at different time periods as described in our earlier publication [51]. An inverted fluorescent microscope (Olympus, FV300) was used to capture the images. The MTT assay was performed according to the reported protocol [52] after five days to determine the viability of cells cultured on the scaffolds as well as to understand the cytotoxicity of the scaffold to cells, if any. Each experiment was performed in triplicates and the results were reported as mean  $\pm$  standard deviation (SD).

## 2.6. Subcutaneous implantation of scaffolds in rats

Before implantation, the PCL membranes were cut into  $1\text{ cm} \times 1\text{ cm}$  and sterilized using ethylene oxide (EtO) vapors. Animal experiments were designed and carried out as recommended in ISO 10993- Part 6 (2016) with the approval of the Institutional animal ethics committee of the host institution (Standard, I. Biological Evaluation of Medical Devices. Part 6. Tests for Local Effects after Implantation; ISO 10993-6; Association for the Advancement of Medical Instrumentation: Arlington, VA, 2016. Int Stand ISO 10993-6 Biol Eval Med devices - Part 6 Tests Local Effects implantation. 2016; 3 ed.). Adult male Sprague Dawley rats weighing  $300 \pm 50\text{ gm}$  were used for the study. The rats were provided with standard environmental controlled conditions of  $25 \pm 3\text{ }^{\circ}\text{C}$ , 12 h light-dark cycle, standard laboratory animal feed (Krish Scientist's Shoppe, Bangalore), and UV-sterile water. A total 8 rats were randomized into 2 groups ( $n = 4$ ) for subcutaneous implantation of scaffolds, with (various DNS concentrations) and without (Blank) DNS. Each animal received one set of all the five scaffolds (PCL, PCL-DNS-0.5, PCL-DNS-1, PCL-DNS-2, and PCL-DNS-4).

On the day of surgery, rats were anesthetized by intramuscular injection of 5 % Xylazine (10 mg/kg of the body weight) and 10 % ketamine hydrochloride (80 mg/kg of the body weight). Hairs at the dorsum of the rats were shaved with Philips electric pet care trimmer and skin was cleaned using 2 % povidone-iodine solution. A linear incision of 8 mm length was made on the dorsal side of the rat using carbon steel surgical blade No. 15 and the full-thickness flap was elevated. All five sterile scaffolds were implanted and fixed using absorbable 3-0 catgut suture and were closed by giving interrupted sutures with number 3-0 black braided silk. In post-operative care, for three days, ceftriaxone (20 mg/kg) and meloxicam (0.5 mg/kg) were administered intramuscular (IM) injection as an antibiotic and analgesic, respectively. The implanted scaffold samples were harvested by euthanizing four rats from each group in a  $\text{CO}_2$  chamber at the first week and fourth weeks of implantation. The connective tissue surrounding scaffolds was fixed in 10 % formalin for histological evaluation. All sections were stained with Harris's hematoxylin and eosin (H&E) stain for histological analysis. After H&E staining, sections were investigated histologically by observing under a polarized optical microscope (Leica DM 4500 P LED) and the images were captured. The sections were viewed and scored by a blinded pathologist using a 4-point scoring system (0 absent, + mild, ++ moderate, and +++ severe) to determine the tissue reaction and membrane degradation.

## 2.7. Statistical analysis

All the experiments were conducted for minimum 3 times. The average values of results were obtained and expressed as mean  $\pm$  S.D. Un-paired Student's t-test was performed between groups of comparison using Graph-Pad QuickCalcs (<https://www.graphpad.com/quickcalcs/ttest1.cfm>).  $P \leq 0.05$  was taken as statistically significant.

## 3. Results and discussion

### 3.1. Characterization of DNS

The morphology of the DNS was investigated by TEM analysis (Fig. 1A and 1B). TEM images at low magnification indicated that the individual DNS particles were with irregular morphology and have width or length in the range of 50–550 nm (Fig. 1A). However, the TEM image illustrates the very transparent feature of the DNS, demonstrating the ultrathin thickness of the nanosheets, whereas the darker portion in the TEM image can be ascribed to the overlap of several DNS nanosheets or a multilayer nanosheet (Fig. 1B). The lattice constant was estimated from the high-resolution TEM images and is  $2.14\text{ }\text{\AA}$  (Fig. 1C). A relatively similar lattice fringe was reported by other researchers also [53]. The electron diffraction pattern shows (111), (220) and (311) crystal

planes of diamond which ascertained the polycrystalline nature of the DNS [54] (Fig. 1D).

Phase and structure of the as-synthesized products were characterized using XRD and FTIR analyses. Fig. 1E shows the XRD pattern of DNS, exhibiting peaks at  $43.9^{\circ}$  and  $75.4^{\circ}$ , indexed to the diffraction from (111) and (220) crystal planes of diamond, respectively [55]. The full width at half maxima (FWHM) of (111) crystal plane of DNS was  $0.1440^{\circ}$  ( $2\theta$ ) with a d-spacing of  $2.05\text{ }\text{\AA}$ . The broadening of the peak is attributed to finite crystallite size and lattice strain. FTIR spectrum provided in Fig. 1F shows the transmittance of DNS, indicating high optical transparency in the near infra-red region.

### 3.2. Morphological and physical characterization of PCL-DNS nanocomposite scaffolds

#### 3.2.1. Morphology

Fig. 2A shows the major technical features of the airbrush spraying device. The polymer solutions were taken in the polymer reservoir and the compressed air was connected through the bottom inlet. The screw at the right side of the device can be adjusted to control polymer flow during spinning. When the flow controller was pressed backward, the compressed air pushed the polymer solution through channel inside the airbrush and pushed out through the nozzle as submicron fibers. The fibers coming out from the nozzles were collected on a flat surface (Fig. 2B). Dried scaffolds were peeled out from the collecting platform and used for various physicochemical and biological characterizations. The obtained scaffolds were very flexible with almost uniform thickness (Fig. 2C). The fabrication process by air-jet spinning was very fast compared to electrospinning and scaffolds with 2 mm thick,  $10\text{ cm} \times 10\text{ cm}$  size were obtained within 20 min of air-jet spinning. However, it takes several hours of spinning to fabricate a scaffold of comparable thickness by electrospinning. For instance, Bhattacharjee et al. reported that an 8 h continuous electrospinning was required to generate 1 mm thick PCL/silk fibroin blended scaffolds [56]. Most other researchers reported a solution flow rate of  $1\text{--}2\text{ mLh}^{-1}$ , obviously taking about 5–10 h to complete the electrospinning of the 10 mL polymer solution [56–60]. In the current work, a 10 mL polymer solution was completely spun within 20 min by air-jet spinning approach.

Surface morphology and diameter of PCL fibres were observed and analysed by SEM and image J software. SEM micrographs of air-jet spun neat PCL scaffolds and PCL-DNS nanocomposite scaffolds are presented in Fig. 2D. It is clearly seen that all the fibres showed almost uniform surface morphology without considerable irregularities. From, Fig. 2 the average fibre diameter of the PCL is estimated to be 322 nm. The average fibre diameter of PCL-DNS-0.5 and PCL-DNS-1 increased slightly, compared to the PCL scaffolds. But PCL-DNS-2 and PCL-DNS-4 have much larger fibre diameters than bare PCL, PCL-DNS-0.5, and PCL-DNS-1. Observed minor variation in fiber diameters can be attributed to the changes in solution properties upon the addition of DNS.

#### 3.2.2. Physical properties of the scaffolds

After DNS was incorporated into the PCL matrix, the XRD patterns of the PCL-DNS composites scaffolds containing lower concentration of DNS were almost the same as those for pure PCL (Fig. 3A). The absence of the characteristic diffraction peak of DNS may clearly demonstrate that DNS is fully dispersed in the PCL matrix. A similar observation was reported in the case of nano diamond incorporated polyimide nanocomposites [61]. However, at higher concentration (PCL-DNS-4), characteristic diffraction patterns of DNS were observed along with the patterns of PCL. From the FTIR analysis, we did not observe any considerable variation of peak positions or emergence of new peaks in the spectra of PCL-DNS nanocomposite scaffolds (Fig. 3B). This result indicates the absence of possible chemical interactions between the functional groups in PCL and DNS.

DSC analysis was performed to investigate the effects of DNS on the crystallization behaviour of the PCL polymer matrix. DSC thermograms

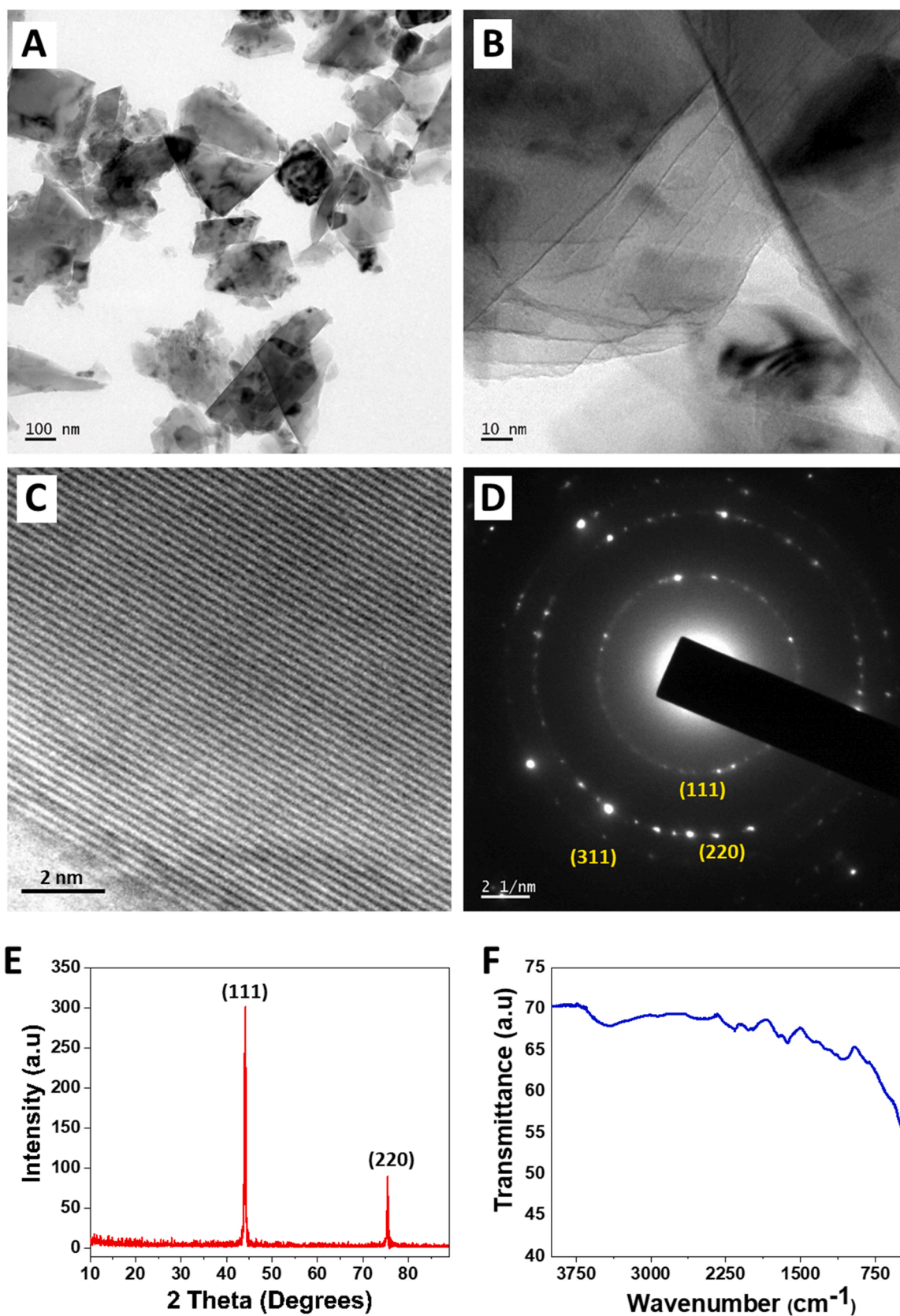


**Fig. 1.** Morphological and physical characterization of DNS used in this study. Transmission electron microscopic (TEM) images of DNS showing the morphology at low (A) and high (B) magnifications. High resolution TEM image, displaying lattice fringes with an interspacing of 0.214 nm (C) and SAED patterns of DNS indicating the polycrystalline nature of DNS (D). XRD pattern (E) and FTIR spectrum (F) of the synthesized DNS.

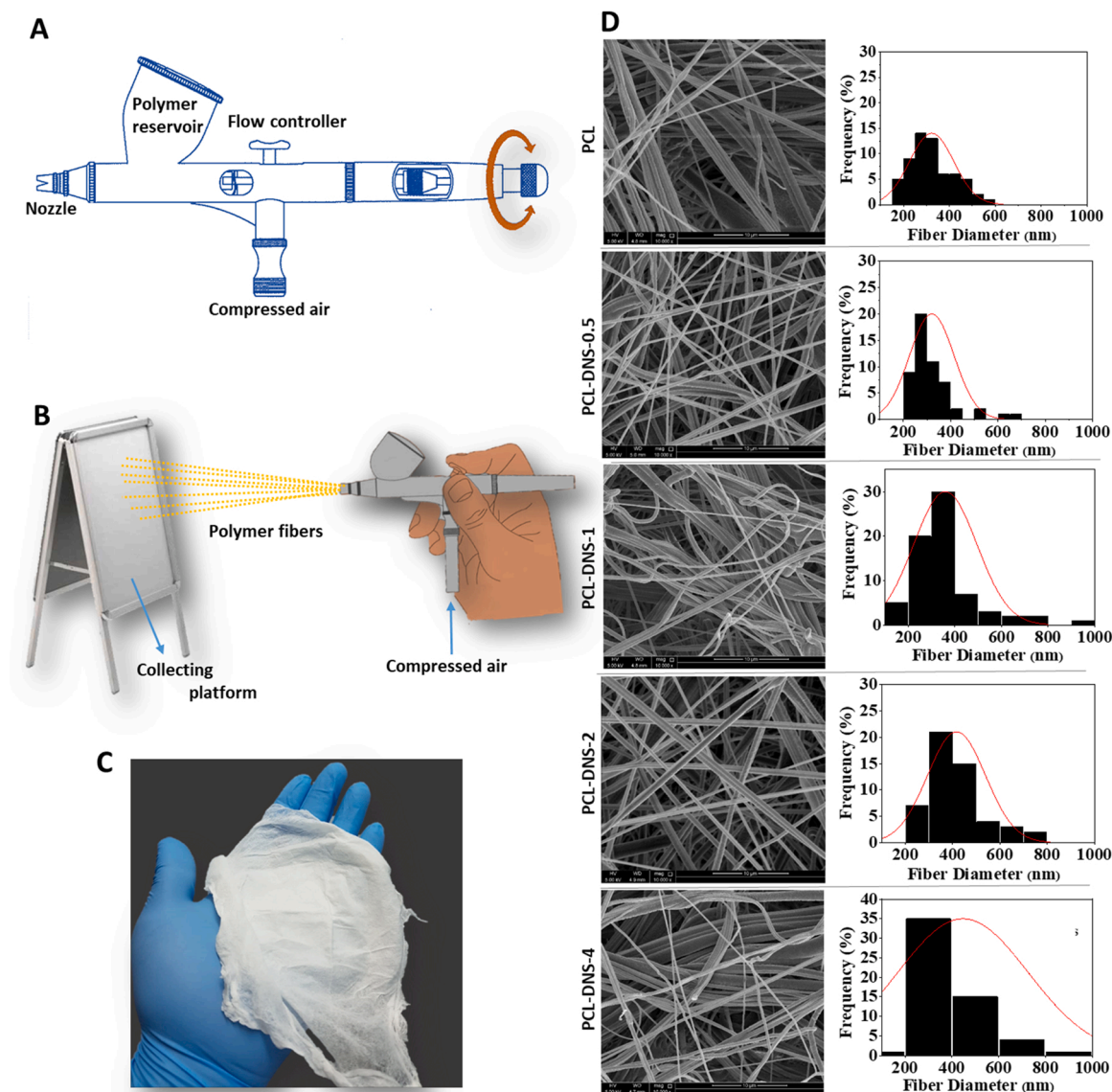


**Fig. 2.** Scheme showing the details of airbrush used for the scaffold fabrication (A). Scheme showing air-jet spinning process (B). Photograph of PCL scaffold fabricated by air-jet spinning process (C). Scanning electron microscopic (SEM) images and fibre diameter distribution graphs of PCL, PCL-DNS-0.5, PCL-DNS-1, PCL-DNS-2, and PCL-DNS-4 scaffolds.

of PCL and PCL-DNS nanocomposites with various DNS loadings are shown in Figs. 3C, 3D. The crystallisation temperature ( $T_c$ ), crystallisation enthalpy ( $\Delta H_c$ ), melting temperature ( $T_m$ ), melting enthalpy ( $\Delta H_m$ ) and crystallinity ( $X_c$ ) obtained from the DSC curves are shown in Table 1. Upon the inclusion of DNS, a slight improvement in  $T_c$  was observed. The rise in crystallization temperature may indicate that the DNS acts both as an efficient nucleating agent for the crystallization of PCL and as barriers to the formation of large crystallite, which was also reported for nanodiamond reinforced polyphenylene sulfide nanocomposites [62]. Melting temperature of PCL membranes did not change significantly whereas  $\Delta H_m$  increased at 0.5 % w/w loading which led to the increase in degree of crystallinity ( $X_c$ ). Even though DNS act as efficient nucleating agent, the strong interfacial interaction between PCL and DNS inhibits the macromolecular free movement and thereby marginally inhibited the crystallisation process above 1 % w/w DNS loading. Marginal increase in  $T_m$  was observed for PCL-DNS nanocomposites which could be associated with the changes in the rate of nucleation and overall crystallinity [63,64].

### 3.2.3. Mechanical properties of the scaffolds

The mechanical properties of the scaffolds are the important factors to be carefully considered because the scaffolds should possess satisfactory strength and flexibility when applied on the defects. Uniaxial tensile testing was performed to understand the mechanical properties of air-jet spun scaffolds. Tensile strength, elongation-at-break and Young's modulus of the scaffolds were calculated based on the data extracted from stress-strain curves and the results are displayed in Fig. 4. Notably, tensile strength showed a concentration dependent initial increase followed by a subsequent decrease. Tensile property of the scaffolds was improved with the inclusion of DNS from 2.53 to 3.76 MPa with addition of up to 2 % w/w DNS and then decreased to 2.45 MPa with 4 % w/w DNS. There was no significant variation in the elongation at break of PCL scaffolds upon incorporation of DNS up to 2 % w/w. Neat PCL scaffolds showed 195.8 % elongation before failure. However, the elongation at break of the scaffolds decreased to 138.6 % when the DNS loading was 4 % w/w. It is well established that the inclusion of large quantities of nanofillers into the polymers generally results in a decline of the elongation at break as evident from other studies [65,66]. Young's modulus of the membrane is increased from 3.45 MPa to 4.42 MPa for 2

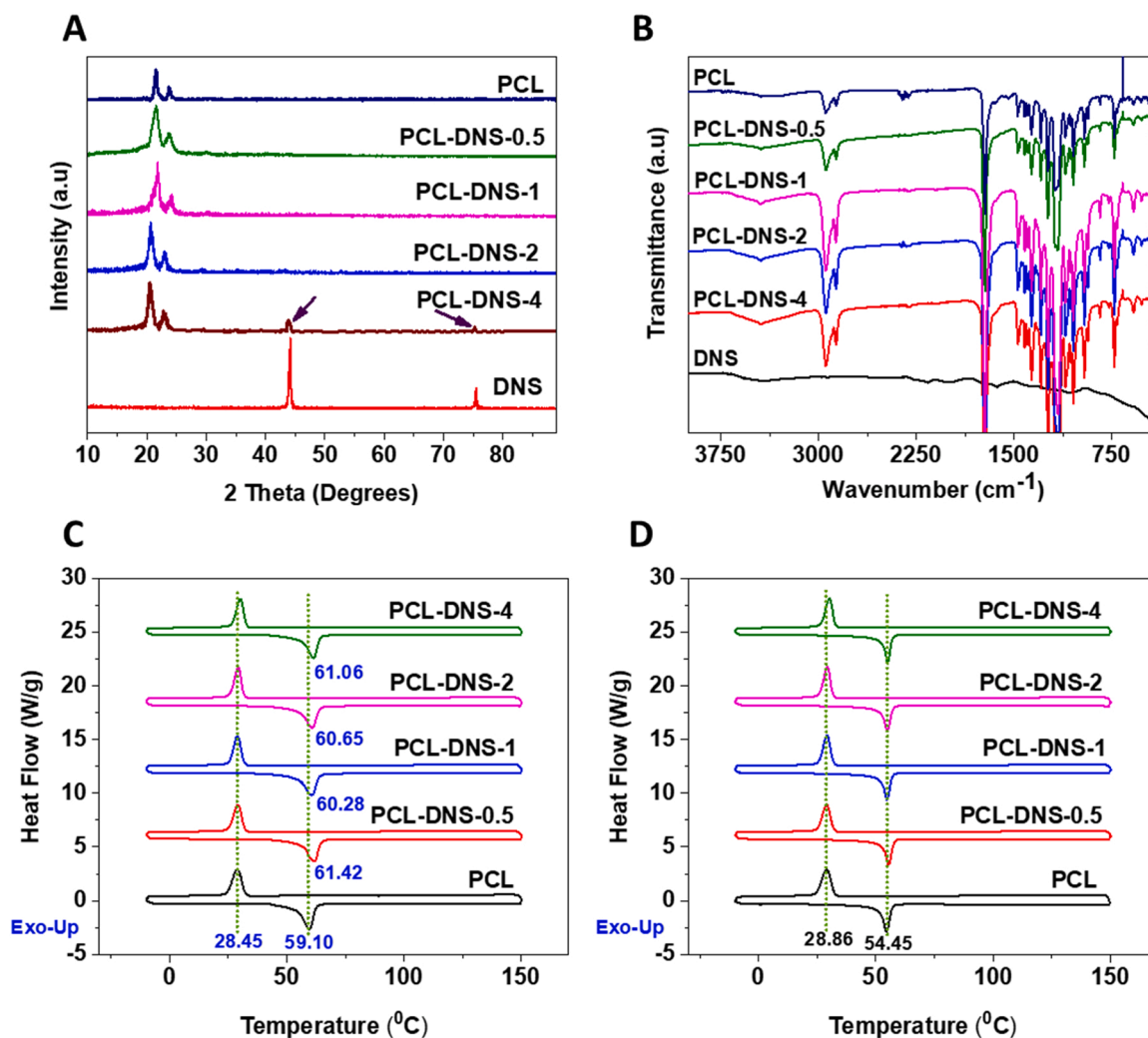


Fig. 3. Physical characterization of the scaffolds. XRD patterns of PCL and PCL-DNS scaffolds (A). FTIR spectra of PCL, and PCL-DNS scaffolds (B). DSC thermograms of PCL and PCL-DNS scaffolds during first heating-cooling cycle (C) and second heating-cooling cycle (D).

Table 1

Effect of DNS on the crystallization temperature (T<sub>c</sub>), melting temperature (T<sub>m</sub>), enthalpy of melting (ΔH<sub>m</sub>), enthalpy of crystallization (ΔH<sub>c</sub>) and degree of crystallinity (X<sub>c</sub>) of the PCL scaffolds.

Sample	T <sub>c</sub> (°C)	T <sub>m</sub> (°C)	ΔH <sub>c</sub> (J g <sup>-1</sup> )	ΔH <sub>m</sub> (J g <sup>-1</sup> )	X <sub>c</sub> (%)
PCL	28.77	59.10	69.28	89.01	63.80
PCL-DNS-0.5	29.02	61.42	70.11	91.83	65.86
PCL-DNS-1	28.95	60.28	72.48	88.17	63.20
PCL-DNS-2	29.27	60.65	72.22	88.05	63.11
PCL-DNS-4	30.18	61.06	71.71	86.19	61.78

% w/w DNS loading, and then decreased to 2.8 MPa for 4 % w/w of DNS loading. Earlier studies indicated that the uniform dispersion of nanodiamond in the polymer led to significant increase in Young's modulus of the composites [67]. It is apparent that the tensile behaviour reverses at higher DNS content, and all mechanical properties appear to be decreased. This is because nanoparticles have a high surface energy and are easily agglomerated, resulting in low dispersion in the polymer matrix. Such agglomerated particles formed in the polymer matrix served as stress concentration centres, preventing stress transfer from the polymer matrix to the fillers, acting as break points, and finally decreasing overall mechanical properties. Moreover, the decreased crystallinity of PCL upon incorporation of 4 % w/w DNS (Refer Table 1) might also have contributed towards the lower mechanical properties of

the scaffolds [68].

### 3.3. Biological performance of the scaffolds

#### 3.3.1. Cell proliferation and viability study on PCL and PCL-DNS scaffolds

Cell proliferation in the presence of PCL-DNS samples was examined on day-1, as well as on day-5, and the results are shown in Fig. 5-A. The cell seeded wells without any scaffolds were used as controls for the comparison. After one day of sample treatment, it was observed that the fibroblasts could cover about 18 % of the surface. As expected, the fibroblast cells showed their characteristic spindle-shaped morphology. Afterward, fibroblast proliferation and division continued gradually on the plates irrespective of DNS loading, reaching a confluency of about 75 % within five-days. The cells would continue to proliferate until confluence, when there would be no more available surface area on the constructs for further cell proliferation. HaCaT keratinocytes also showed a similar pattern of proliferation in the presences of PCL scaffolds containing various amounts of DNS (Fig. 5B). We observed a relatively small number of dead cells upon treatment with PCL-DNS composite scaffolds, especially above 1 % w/w DNS content. However, various studies using nanodiamonds reported different results with respect to cytocompatibility and cell viability. Such variations obviously be related to differences in surface functional groups in nanodiamonds generated by different processes. For instance, oxygen-terminated nanodiamonds, the cell viability and the cell number remained almost

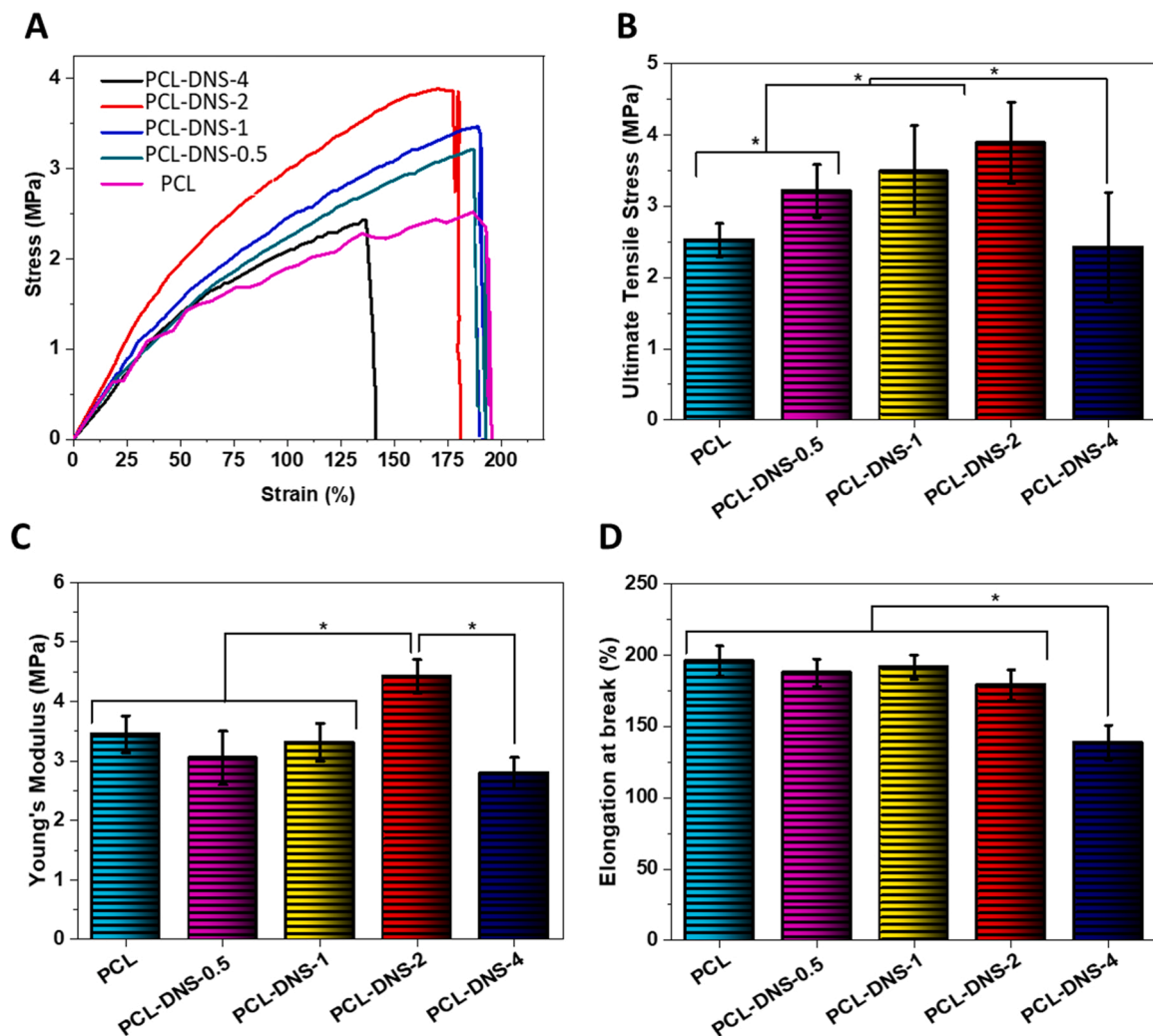


**Fig. 4.** Tensile mechanical properties of developed scaffolds. Stress-strain curves (A), Ultimate Tensile Stress (B), Elongation at break (C) and Young's Modulus obtained from the tensile testing of neat PCL and PCL-DNS nanocomposite scaffolds.

the same for concentrations up to 100  $\mu\text{g/mL}$  [69]. However, the hydrogen-terminated detonation nanodiamonds caused about 15–20 % reduction in the cell viability and cell number. By considering such factors, detailed investigations based on the surface functional groups on DNSs need to be performed before making conclusive remarks regarding the concentration dependent effect of DNSs loaded PCL scaffolds on cell viability. Moreover, different types of cells show difference in cellular response upon culturing with nanodiamonds. For instance, unlike the cancer cells, nanodiamonds did not affect the cell cycle progression and cell proliferation associated gene expression in normal cells [70]. Therefore, we also intend to conduct experimental studies to understand the cell type-dependent variation of cell viability upon culturing with PCL-DNS scaffolds.

Results from the MTT cell viability assay are provided in Fig. 5C & D. The findings obtained for 3T3 fibroblasts (Fig. 5C) and HaCaT keratinocytes (Fig. 5D), suggest that the incorporation of DNS on the scaffold had no cytotoxic effect on the cells.

From these experimental data, the air-jet spun PCL-DNS scaffolds can be considered as a robust biomaterial scaffold for various tissue engineering applications, that can provide a comparable cell proliferation with that of blank PCL scaffolds. Additional strategies such as coating of PCL-DNS scaffolds with bioactive natural polymers such as fibronectin, collagen, or gelatin may further improve the cell proliferation while maintaining the advantage of increased mechanical strength due to the incorporation of DNS.

### 3.3.2. *In vivo biocompatibility of the scaffolds*

The local tissue reaction after subcutaneous implantation of the scaffolds for four weeks in rats was analysed through histopathological analysis. Throughout the implantation experiment, all the animals were physically stable, and no deaths were observed. The scaffolds did not elicit any visually detectable adverse effects, according to the visual inspection of the implantation site and explanted scaffolds (Fig. 6A). Interestingly, PCL-DNS scaffolds supported blood vessel formation especially after one week of implantation as evident from the presence of RBCs (Pink/red cells) (Fig. 6B). The highest angiogenic responses were observed with PCL-DNS-2 scaffolds during the study period which needs further investigation to elucidate the underlying mechanism.

Inflammatory responses upon implantation of the scaffolds were also measured and presented in supplementary information Table S1-S4. In H&E-stained portions of implanted scaffolds, no adverse chronic inflammatory responses were found. Explanted tissues lacked acute inflammation, abscess formation, and tissue necrosis. In the case of PCL scaffolds, there were only a few multinucleated giant cells around the implant; however, slightly higher number of multinucleated giant cells were present in the case of PCL-DNS scaffolds. As a result, these scaffolds showed a low to moderate tissue response, with lymphocytes, macrophages, fibroblasts, and a few giant cells. PMNs (polymorphonuclear leukocytes) were uncommon. At the end of four weeks of implantation, PCL-DNS scaffolds had a higher number of fibroblast cells. PCL-DNS-4 scaffolds, on the other hand, had a higher number of giant cells and

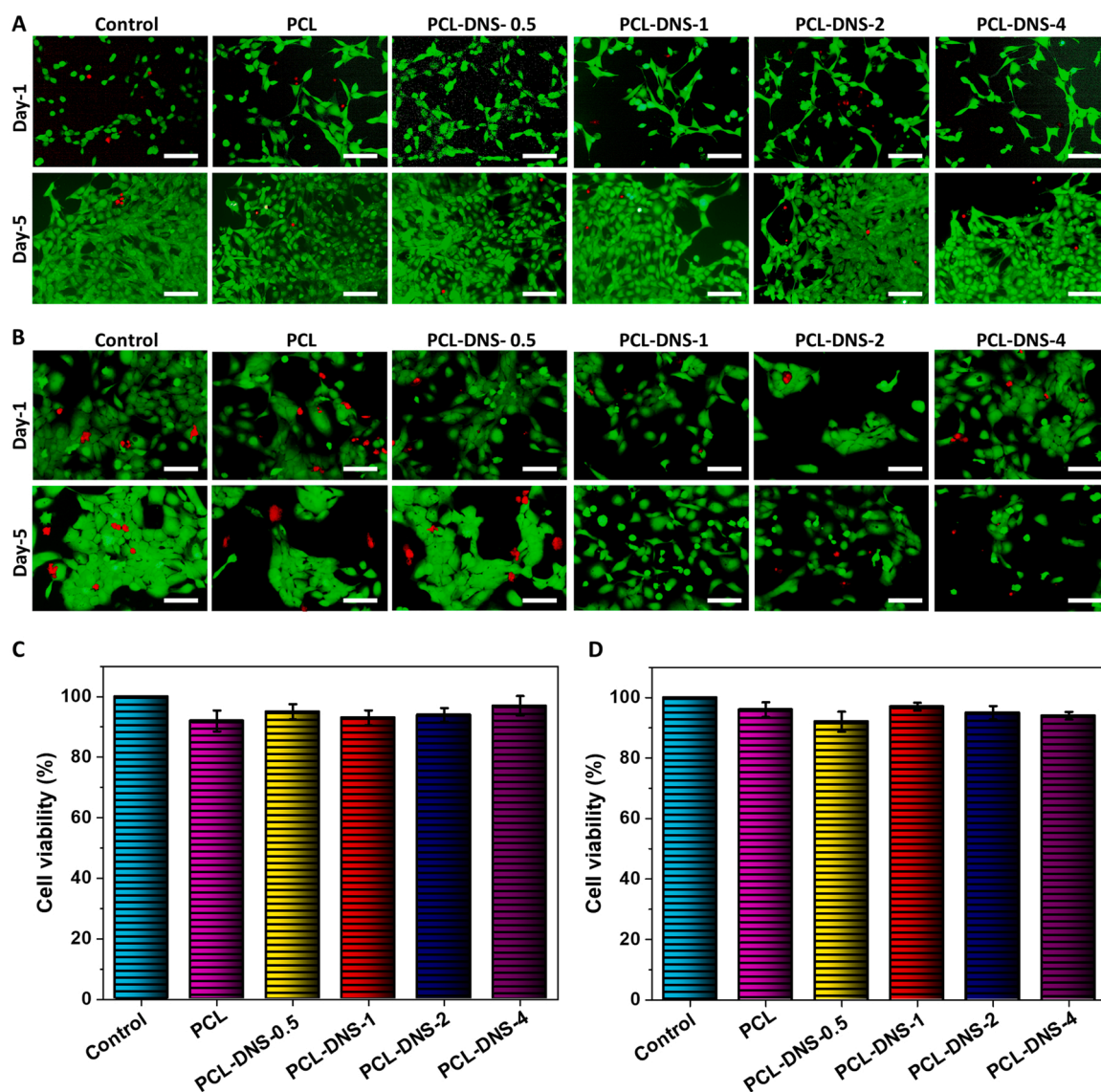


**Fig. 5.** 3T3 fibroblast (A) and HaCaT keratinocyte (B) cell morphology after 1, and 5 days of culture on tissue culture plates containing scaffolds. MTT cell viability assay performed using 3T3 fibroblasts (B) and HaCaT keratinocytes (C) treated with the scaffolds. Scale bars = 200 μm.

PMNs. Despite, the minor differences in the inflammatory response at higher concentration of DNS, none of the nanocomposite scaffolds showed considerable adverse effects. Hence, based on the histopathological evaluation and as evident from previous studies [71], incorporation of diamond nanosheets in PCL scaffolds is a safe strategy to improve the material properties.

Developing highly porous but mechanically strong tissue engineering scaffolds that could lead to a better mechanical compatibility with implantation site and result in a better outcome. A air-jet spinning is an excellent technique to generate highly porous submicron fibrous scaffolds. When DNS were dispersed homogeneously in PCL polymer matrix, the mechanical strength of the scaffolds increased significantly. Unlike many other nanofillers, DNS did not affect cell proliferation or cell viability even at 4 % w/w loading in the scaffolds. Animal implantation studies in rats showed that PCL-DNS scaffolds are able to integrate well with surrounding host tissue, without producing considerable local inflammatory response. These superior mechanical properties and biocompatibility of air-jet spun DNS loaded PCL scaffolds indicate that they can be used as cell supportive scaffolds for wide range of tissue engineering applications.

#### 4. Conclusions

PCL based tissue engineering scaffolds containing DNS were successfully fabricated by using the air-jet spinning technique. The DNS loaded PCL scaffolds showed submicron/microfibres with relatively uniform fibre morphology and adequate mechanical properties. Interestingly, it was observed that the PCL-DNS scaffolds had significantly high values of both Young's modulus and ultimate tensile strength. As expected, PCL-DNS scaffolds were highly cytocompatible and supported mammalian cell growth *in vitro*. Subcutaneous implantation of the scaffolds in rats supported the *in vitro* results. PCL-DNS scaffolds did not produce considerable tissue response in rats up to 2 % w/w DNS loading. Overall, this research indicates that air-jet spun PCL scaffolds loaded with an appropriate concentration of DNS could be considered as excellent scaffolds for a wide range of tissue engineering applications.

#### CRediT authorship contribution statement

**Robin Augustine:** Conceptualization, Methodology, Formal analysis, Visualization, Writing – original draft, Writing – review & editing, Validation, Project administration, Supervision. **Sumama Nuthana**

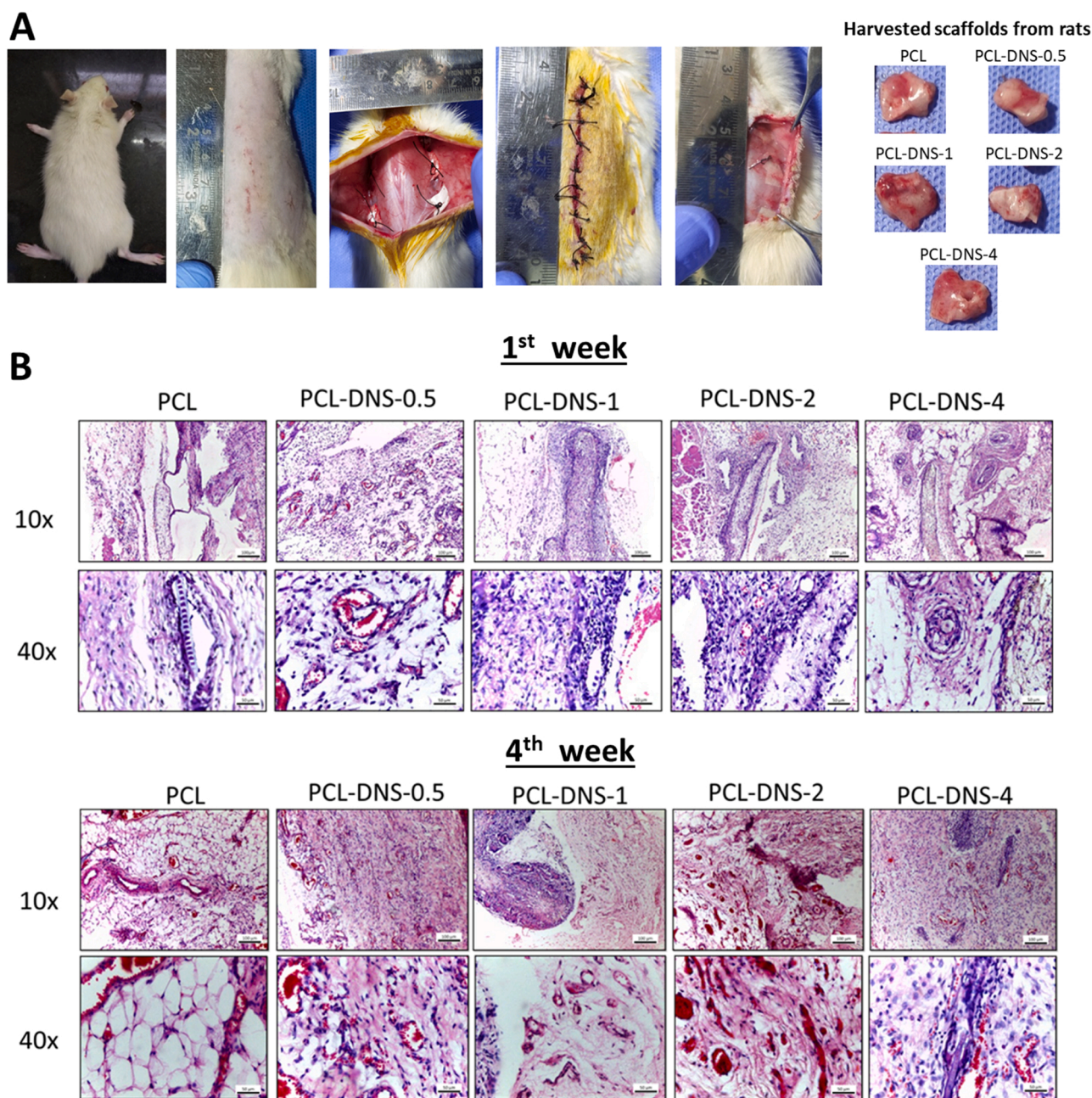


**Fig. 6.** Digital photographs showing the implantation and harvesting scaffolds with infiltrated tissue for histological analysis (A). Micrographs of H&E-stained PCL and PCL-DNS scaffolds implanted for one and four weeks showing the cell proliferation, angiogenesis, and tissue response if any. Images were taken using 10x (Scale bars = 100  $\mu$ m) and 40x (Scale bars = 50  $\mu$ m) objective lenses.

**Kalva:** Methodology, Formal analysis, Visualization, Validation, Writing - review & editing. **Yogesh B. Dalvi:** Methodology, Formal analysis, Writing - review & editing. **Ruby Varghese:** Methodology, Writing - review & editing. **Maneesh Chandran:** Methodology, Writing - review & editing. **Anwarul Hasan:** Project administration, Funding acquisition, Supervision, Validation, Writing - review & editing.

#### Declaration of Competing Interest

The authors declare that they have no known competing financial interests or personal relationships that could have appeared to influence the work reported in this paper.

#### Data Availability

Data will be made available on request.

#### Acknowledgments

This article was made possible by the NPRP12S-0310-190276 grant funded by the Qatar National Research Fund (a part of the Qatar Foundation). We also acknowledge the support provided by the Center for Advanced Materials (CAM) and Central Laboratories Unit (CLU), Qatar University, Qatar.

## Appendix A. Supporting information

Supplementary data associated with this article can be found in the online version at [doi:10.1016/j.colsurfb.2022.112958](https://doi.org/10.1016/j.colsurfb.2022.112958).

## References

- [1] L. Shahzadi, R. Zeeshan, M. Yar, S. Bin Qasim, A.A. Chaudhry, A.F. Khan, N. Muhammad, Biocompatibility through cell attachment and cell proliferation studies of Nylon 6/Chitosan/Ha electrospun mats, *J. Polym. Environ.* 26 (2018) 2030–2038, <https://doi.org/10.1007/S10924-017-1100-8/FIGURES/8>.
- [2] A.S. Khan, A.N. Hussain, L. Sidra, Z. Sarfraz, H. Khalid, M. Khan, F. Manzoor, L. Shahzadi, M. Yar, I.U. Rehman, Fabrication and in vivo evaluation of hydroxyapatite/carbon nanotube electrospun fibers for biomedical/dental application, *Mater. Sci. Eng. C* 80 (2017) 387–396, <https://doi.org/10.1016/j.msec.2017.05.109>.
- [3] R. Augustine, P. Dan, I. Schlachet, D. Rouxel, P. Menu, A. Sosnik, Chitosan ascorbate hydrogel improves water uptake capacity and cell adhesion of electrospun poly(epsilon-caprolactone) membranes, *Int. J. Pharm.* 559 (2019), <https://doi.org/10.1016/j.ijpharm.2019.01.063>.
- [4] A.A. Zahid, R. Ahmed, S. Raza ur Rehman, R. Augustine, M. Tariq, A. Hasan, Nitric oxide releasing chitosan-poly (vinyl alcohol) hydrogel promotes angiogenesis in chick embryo model, *Int. J. Biol. Macromol.* 136 (2019), <https://doi.org/10.1016/j.ijbiomac.2019.06.136>.
- [5] S. Shahzad, M. Yar, S.A. Siddiqi, N. Mahmood, A. Rauf, Z. ul A. Qureshi, M. S. Anwar, S. Afzaal, Chitosan-based electrospun nanofibrous mats, hydrogels and cast films: novel anti-bacterial wound dressing matrices, *J. Mater. Sci. Mater. Med.* 26 (2015) 1–12, <https://doi.org/10.1007/s10856-015-5462-y>.
- [6] A. Abdal-Hay, N.A.M. Barakat, J.K. Lim, Novel technique for polymeric nanofibers preparation: air jet spinning, *Sci. Adv. Mater.* 4 (2012) 1268–1275, <https://doi.org/10.1166/sam.2012.1382>.
- [7] A. Abdal-Hay, A.S. Hamdy Makhlof, K.A. Khalil, Novel, facile, single-step technique of polymer/TiO<sub>2</sub> nanofiber composites membrane for photodegradation of methylene blue, *ACS Appl. Mater. Interfaces* 7 (2015) 13329–13341, <https://doi.org/10.1021/acsami.5b01418>.
- [8] A. Abdal-Hay, F.A. Sheikh, J.K. Lim, Air jet spinning of hydroxyapatite/poly(lactic acid) hybrid nanocomposite membrane mats for bone tissue engineering, *Colloids Surf. B Biointerfaces* 102 (2013) 635–643, <https://doi.org/10.1016/j.colsurfb.2012.09.017>.
- [9] A. Abdal-Hay, Y.S. Oh, A. Yousef, H.R. Pant, P. Vanegas, J.K. Lim, In vitro deposition of Ca-P nanoparticles on air jet spinning Nylon 6 nanofibers scaffold for bone tissue engineering, *Appl. Surf. Sci.* 307 (2014) 69–76, <https://doi.org/10.1016/j.apsusc.2014.03.161>.
- [10] M.V. Granados-Hernández, J. Serrano-Bello, J.J. Montesinos, C. Alvarez-Gayosso, L.A. Medina-Velázquez, O. Alvarez-Fregoso, M.A. Alvarez-Perez, In vitro and in vivo biological characterization of poly(lactic acid) fiber scaffolds synthesized by air jet spinning, *J. Biomed. Mater. Res B Appl. Biomater.* 106 (2018) 2435–2446, <https://doi.org/10.1002/jbm.b.34053>.
- [11] A. Abdal-Hay, F.A. Sheikh, J.K. Lim, Air jet spinning of hydroxyapatite/poly(lactic acid) hybrid nanocomposite membrane mats for bone tissue engineering, *Colloids Surf. B Biointerfaces* 102 (2013) 635–643, <https://doi.org/10.1016/j.colsurfb.2012.09.017>.
- [12] A. Abdal-Hay, N.A.M. Barakat, J.K. Lim, Novel technique for polymeric nanofibers preparation: air jet spinning, *Sci. Adv. Mater.* 4 (2012) 1268–1275, <https://doi.org/10.1166/sam.2012.1382>.
- [13] K. Ghosal, R. Augustine, A. Zaszczynska, M. Barman, A. Jain, A. Hasan, N. Kalarikkal, P. Sajkiewicz, S. Thomas, Novel drug delivery systems based on triaxial electrospinning based nanofibers, *React. Funct. Polym.* 163 (2021), 104895, <https://doi.org/10.1016/j.reactfunctpolym.2021.104895>.
- [14] M. Yar, G. Gigliobianco, L. Shahzadi, L. Dew, S.A. Siddiqi, A.F. Khan, A. Chaudhry, I.U. Rehman, S. MacNeil, Production of chitosan PVA PCL hydrogels to bind heparin and induce angiogenesis, *Int. J. Polym. Mater. Polym. Biomater.* 65 (2016) 466–476, <https://doi.org/10.1080/00914037.2015.1129959>.
- [15] R. Augustine, A. Hasan, N.K. Patan, A. Augustine, Y.B. Dalvi, R. Varghese, R. N. Unni, N. Kalarikkal, A.E. Al Moustafa, S. Thomas, Titanium nanorods loaded PCL meshes with enhanced blood vessel formation and cell migration for wound dressing applications, *Macromol. Biosci.* 24 (2019) 101–123, <https://doi.org/10.1002/mabi.201900058>.
- [16] R. Augustine, Y.B. Dalvi, V.K. Yadu Nath, R. Varghese, V. Raghuvveeran, A. Hasan, S. Thomas, N. Sandhyarani, Yttrium oxide nanoparticle loaded scaffolds with enhanced cell adhesion and vascularization for tissue engineering applications, *Mater. Sci. Eng. C* 103 (2019), 109801, <https://doi.org/10.1016/j.msec.2019.109801>.
- [17] R. Augustine, S.R. ur Rehman, J.K.S., A. Hasan, Stromal cell-derived factor loaded co-electrospun hydrophilic/hydrophobic bicomponent membranes for wound protection and healing, *RSC Adv.* 11 (2021) 572–583, <https://doi.org/10.1039/d0ra04997b>.
- [18] A. Hasan, S. Soliman, F. El Hajj, Y.T. Tseng, H.C. Yalcin, H.E. Marei, Fabrication and in vitro characterization of a tissue engineered PCL-PLLA heart valve, *Sci. Rep.* 8 (2018) 8187, <https://doi.org/10.1038/s41598-018-26452-y>.
- [19] R. Augustine, S.K. Nethi, N. Kalarikkal, S. Thomas, C.R. Patra, Electrospun polycaprolactone (PCL) scaffolds embedded with europium hydroxide nanorods (EHNs) with enhanced vascularization and cell proliferation for tissue engineering applications, *J. Mater. Chem. B* 5 (2017) 4660–4672, <https://doi.org/10.1039/c7tb00518k>.
- [20] R. Augustine, E.A. Dominic, I. Reju, B. Kaimal, N. Kalarikkal, S. Thomas, Electrospun polycaprolactone membranes incorporated with ZnO nanoparticles as skin substitutes with enhanced fibroblast proliferation and wound healing, *RSC Adv.* 4 (2014) 24777–24785, <https://doi.org/10.1039/C4RA02450H>.
- [21] S. Ahtaz, M. Nasir, L. Shahzadi, F. Iqbal, A.A. Chaudhry, M. Yar, I. ur Rehman, W. Amir, A. Anjum, R. Arshad, A study on the effect of zinc oxide and zinc peroxide nanoparticles to enhance angiogenesis-pro-angiogenic grafts for tissue regeneration applications, *Mater. Des.* 132 (2017) 409–418, <https://doi.org/10.1016/j.matdes.2017.07.023>.
- [22] S. Das, J.M. Dowding, K.E. Klump, J.F. McGinnis, W. Self, S. Seal, Cerium oxide nanoparticles: applications and prospects in nanomedicine, *Nanomedicine* (2013), <https://doi.org/10.2217/nmm.13.133>.
- [23] R. Augustine, Y.B. Dalvi, P. Dan, N. George, D. Helle, R. Varghese, S. Thomas, P. Menu, N. Sandhyarani, Nanoceria can act as the cues for angiogenesis in tissue-engineering scaffolds: toward next-generation in situ tissue engineering, *ACS Biomater. Sci. Eng.* 4 (2018) 4338–4353, <https://doi.org/10.1021/acsbomaterials.8b01102>.
- [24] R. Augustine, A.A. Zahid, A. Hasan, Y.B. Dalvi, J. Jacob, Cerium oxide nanoparticle-loaded gelatin methacryloyl hydrogel wound-healing patch with free radical scavenging activity, *ACS Biomater. Sci. Eng.* 7 (2021) 279–290, <https://doi.org/10.1021/acsbomaterials.0c01138>.
- [25] S. Kargozar, F. Baino, S.J. Hoseini, S. Hamzehlou, M. Darroudi, J. Verdi, L. Hasanazadeh, H.W. Kim, M. Mozafari, Biomedical applications of nanoceria: new roles for an old player, *Nanomedicine* 13 (2018) 3051–3069, <https://doi.org/10.2217/nmm-2018-0189>.
- [26] R. Augustine, S.K. Nethi, N. Kalarikkal, S. Thomas, C.R. Patra, Electrospun polycaprolactone (PCL) scaffolds embedded with europium hydroxide nanorods (EHNs) with enhanced vascularization and cell proliferation for tissue engineering applications, *J. Mater. Chem. B* 5 (2017) 4660–4672, <https://doi.org/10.1039/c7tb00518k>.
- [27] M. Ghadiri, W. Chrzanowski, R. Rohanizadeh, Biomedical applications of cationic clay minerals, *RSC Adv.* (2015), <https://doi.org/10.1039/c4ra16945j>.
- [28] S. Kargozar, M. Mozafari, S. Ghodrati, E. Fiume, F. Baino, Copper-containing bioactive glasses and glass-ceramics: from tissue regeneration to cancer therapeutic strategies, *Mater. Sci. Eng. C* 121 (2021), 111741, <https://doi.org/10.1016/j.msec.2020.111741>.
- [29] T. Lu, L. Wang, Y. Jiang, Q. Liu, C. Huang, Hexagonal boron nitride nanoplates as emerging biological nanovectors and their potential applications in biomedicine, *J. Mater. Chem. B* (2016), <https://doi.org/10.1039/c6tb01481j>.
- [30] Y. Kuthati, R.K. Kankala, C.-H. Lee, Layered double hydroxide nanoparticles for biomedical applications: Current status and recent prospects, *Appl. Clay Sci.* (2015), <https://doi.org/10.1016/j.clay.2015.04.018>.
- [31] R. Kumar, V.B. Kumar, A. Gedanken, Sonochemical synthesis of carbon dots, mechanism, effect of parameters, and catalytic, energy, biomedical and tissue engineering applications, *Ultrason. Sonochem.* 64 (2020), 105009, <https://doi.org/10.1016/j.ultrasonch.2020.105009>.
- [32] S. Kargozar, S.J. Hoseini, P.B. Milan, S. Hooshmand, H.W. Kim, M. Mozafari, Quantum dots: a review from concept to clinic, *Biotechnol. J.* 15 (2020) 2000117, <https://doi.org/10.1002/biot.202000117>.
- [33] X. Liu, M.N. George, L. Li, D. Gamble, A.L. Miller, B. Gaihr, B.E. Waletzki, L. Lu, Injectable electrical conductive and phosphate releasing gel with two-dimensional black phosphorus and carbon nanotubes for bone tissue engineering, *ACS Biomater. Sci. Eng.* 6 (2020) 4653–4665, <https://doi.org/10.1021/acsbomaterials.0c00612>.
- [34] S.R. ur Rehman, R. Augustine, A.A. Zahid, R. Ahmed, M. Tariq, A. Hasan, Reduced graphene oxide incorporated gelma hydrogel promotes angiogenesis for wound healing applications, *Int. J. Nanomed.* 14 (2019) 9603–9617, <https://doi.org/10.2147/IJN.S218120>.
- [35] R. Augustine, A. Hasan, R. Primavera, R.J. Wilson, A.S. Thakor, B.D. Kevadiya, Cellular uptake and retention of nanoparticles: insights on particle properties and interaction with cellular components, *Mater. Today Commun.* 25 (2020), 101692, <https://doi.org/10.1016/j.mtcomm.2020.101692>.
- [36] R. Augustine, A. Augustine, N. Kalarikkal, S. Thomas, Fabrication and characterization of biosilver nanoparticles loaded calcium pectinate nano-micro dual-porous antibacterial wound dressings, *Prog. Biomater.* 5 (2016) 223–235, <https://doi.org/10.1007/s40204-016-0060-8>.
- [37] S. Kargozar, M. Mozafari, Nanotechnology and nanomedicine: start small, think big, *Mater. Today Proc.* 5 (2018) 15492–15500, <https://doi.org/10.1016/j.matpr.2018.04.155>.
- [38] A. Nie, Y. Bu, P. Li, Y. Zhang, T. Jin, J. Liu, Z. Su, Y. Wang, J. He, Z. Liu, H. Wang, Y. Tian, W. Yang, Approaching diamond's theoretical elasticity and strength limits, *Nat. Commun.* 10 (2019) 1–7, <https://doi.org/10.1038/s41467-019-13378-w>.
- [39] R.J. Narayan, R.D. Boehm, A.V. Sumant, Medical applications of diamond particles & surfaces, *Mater. Today* 14 (2011) 154–163, [https://doi.org/10.1016/S1369-7021\(11\)70087-6](https://doi.org/10.1016/S1369-7021(11)70087-6).
- [40] A. Kromka, L. Gorausova, L. Bacakova, J. Vacik, B. Rezek, M. Vanecek, O. A. Williams, K. Haenen, Semiconducting to metallic-like boron doping of nanocrystalline diamond films and its effect on osteoblastic cells, *Diam. Relat. Mater.* 19 (2010) 190–195, <https://doi.org/10.1016/j.diamond.2009.10.003>.
- [41] M. Kopecek, L. Bacakova, J. Vacik, F. Fendrych, V. Vorlicek, I. Kratochvilova, V. Lisa, E. Van Hove, C. Mer, P. Bergonzo, M. Nesladek, Improved adhesion, growth and maturation of human bone-derived cells on nanocrystalline diamond films, in: *Physica Status Solidi (A) Applications and Materials Science*, John Wiley & Sons, Ltd, 2008: pp. 2146–2153. <https://doi.org/10.1002/pssa.200879729>.

- [42] A. Broz, V. Baresova, A. Kromka, B. Rezek, M. Kalbacova, Strong influence of hierarchically structured diamond nanotopography on adhesion of human osteoblasts and mesenchymal cells, *Phys. Status Solidi (A) Appl. Mater. Sci.* 206 (2009) 2038–2041, <https://doi.org/10.1002/pssa.200982203>.
- [43] J. Liskova, O. Babchenko, M. Varga, A. Kromka, D. Hadraba, Z. Svindrych, Z. Burdikova, L. Bacakova, Osteogenic cell differentiation on H-terminated and O-terminated nanocrystalline diamond films, *Int. J. Nanomed.* 10 (2015) 869–884, <https://doi.org/10.2147/IJN.S73628>.
- [44] L. Grausova, A. Kromka, Z. Burdikova, A. Eckhardt, B. Rezek, J. Vacik, K. Haenen, V. Lisa, L. Bacakova, Enhanced growth and osteogenic differentiation of human osteoblast-like cells on boron-doped nanocrystalline diamond thin films, *PLoS One* 6 (2011), <https://doi.org/10.1371/journal.pone.0020943>.
- [45] L. Yang, B.W. Sheldon, T.J. Webster, Orthopedic nano diamond coatings: control of surface properties and their impact on osteoblast adhesion and proliferation, *J. Biomed. Mater. Res A* 91 (2009) 548–556, <https://doi.org/10.1002/jbm.a.32227>.
- [46] S. Balakin, Y.S. Yun, J. Lee, E.H. Kang, J. Spohn, I.S. Yun, J. Opitz, G. Cuniberti, J. S. Yeo, In vitro characterization of osteoblast cells on polyelectrolyte multilayers containing detonation nanodiamonds, *Biomed. Mater. (Bristol)* 15 (2020), 055026, <https://doi.org/10.1088/1748-605X/ab9baf>.
- [47] Q. Zhang, V.N. Mochalin, I. Neitzel, I.Y. Knoke, J. Han, C.A. Klug, J.G. Zhou, P. I. Lelkes, Y. Gogotsi, Fluorescent PLLA-nanodiamond composites for bone tissue engineering, *Biomaterials* 32 (2011) 87–94, <https://doi.org/10.1016/j.biomaterials.2010.08.090>.
- [48] Q. Zhang, V.N. Mochalin, I. Neitzel, K. Hazeli, J. Niu, A. Kontsos, J.G. Zhou, P. I. Lelkes, Y. Gogotsi, Mechanical properties and biomineralization of multifunctional nanodiamond-PLLA composites for bone tissue engineering, *Biomaterials* 33 (2012) 5067–5075, <https://doi.org/10.1016/j.biomaterials.2012.03.063>.
- [49] Y. Sun, Q. Yang, H. Wang, Synthesis and characterization of nanodiamond reinforced chitosan for bone tissue engineering, *J. Funct. Biomater.* 7 (2016) 27, <https://doi.org/10.3390/jfb7030027>.
- [50] K. Fox, R. Ratwatt, M.A. Booth, H.M. Tran, P.A. Tran, High nanodiamond content-PCL composite for tissue engineering scaffolds, *Nanomaterials* 10 (2020) 948, <https://doi.org/10.3390/nano10050948>.
- [51] R. Augustine, A. Hasan, Y.B. Dalvi, S.R.U. Rehman, R. Varghese, R.N. Unni, H. C. Yalcin, R. Alifkey, S. Thomas, A.E. Al Moustafa, Growth factor loaded in situ photocrosslinkable poly(3-hydroxybutyrate-co-3-hydroxyvalerate)/gelatin methacryloyl hybrid patch for diabetic wound healing, *Mater. Sci. Eng. C* 118 (2021), 111519, <https://doi.org/10.1016/j.msec.2020.111519>.
- [52] R. Augustine, A. Hasan, Y.B. Dalvi, S.R.U. Rehman, R. Varghese, R.N. Unni, H. C. Yalcin, R. Alifkey, S. Thomas, A.E. Al Moustafa, Growth factor loaded in situ photocrosslinkable poly(3-hydroxybutyrate-co-3-hydroxyvalerate)/gelatin methacryloyl hybrid patch for diabetic wound healing, *Mater. Sci. Eng. C* 118 (2021), 111519, <https://doi.org/10.1016/j.msec.2020.111519>.
- [53] A. Kumar, P. Ann Lin, A. Xue, B. Hao, Y. Khin Yap, R.M. Sankaran, Formation of nanodiamonds at near-ambient conditions via microplasma dissociation of ethanol vapour, *Nat. Commun.* 4 (2013) 2618, <https://doi.org/10.1038/ncomms3618>.
- [54] F. Brunet, A. Deneuville, P. Germe, M. Pernet, E. Gheeraert, J. Mambou, Effect of boron incorporation on the structure of polycrystalline diamond films, *Diam. Relat. Mater.* 6 (1997) 774–777, [https://doi.org/10.1016/s0925-9635\(96\)00607-3](https://doi.org/10.1016/s0925-9635(96)00607-3).
- [55] S. Wang, F. Qin, Y. Bai, D. Zhang, J. Zhang, Impact of the deposition temperature on the structural and electrical properties of INN films grown on self-standing diamond substrates by low-temperature ECR-MOCVD, *Coatings* 10 (2020) 1–11, <https://doi.org/10.3390/coatings10121185>.
- [56] P. Bhattacharjee, D. Naskar, T.K. Maiti, D. Bhattacharya, P. Das, S.K. Nandi, S. C. Kundu, Potential of non-mulberry silk protein fibroin blended and grafted poly( $\epsilon$ -caprolactone) nanofibrous matrices for in vivo bone regeneration, *Colloids Surf. B Biointerfaces* 143 (2016) 431–439, <https://doi.org/10.1016/j.colsurfb.2016.03.058>.
- [57] A. Daghrery, Z. Aytac, N. Dubey, L. Mei, A. Schwendeman, M.C. Bottino, Electrospinning of dexamethasone/cyclodextrin inclusion complex polymer fibers for dental pulp therapy, *Colloids Surf. B Biointerfaces* 191 (2020), 111011, <https://doi.org/10.1016/j.colsurfb.2020.111011>.
- [58] X. Li, Y. Su, S. Liu, L. Tan, X. Mo, S. Ramakrishna, Encapsulation of proteins in poly(L-lactide-co-caprolactone) fibers by emulsion electrospinning, *Colloids Surf. B Biointerfaces* 75 (2010) 418–424, <https://doi.org/10.1016/j.colsurfb.2009.09.014>.
- [59] J. Pasuri, J. Holopainen, H. Kokkonen, M. Persson, K. Kauppinen, P. Lehenkari, E. Santala, M. Ritala, J. Tuukkanen, Osteoclasts in the interface with electrospun hydroxyapatite, *Colloids Surf. B Biointerfaces* 135 (2015) 774–783, <https://doi.org/10.1016/j.colsurfb.2015.08.045>.
- [60] M. Lian, B. Sun, Z. Qiao, K. Zhao, X. Zhou, Q. Zhang, D. Zou, C. He, X. Zhang, Bi-layered electrospun nanofibrous membrane with osteogenic and antibacterial properties for guided bone regeneration, *Colloids Surf. B Biointerfaces* 176 (2019) 219–229, <https://doi.org/10.1016/j.colsurfb.2018.12.071>.
- [61] S. Qin, M. Cui, S. Qiu, H. Zhao, L. Wang, A. Zhang, Dopamine@Nanodiamond as novel reinforcing nanofillers for polyimide with enhanced thermal, mechanical and wear resistance performance, *RSC Adv.* 8 (2018) 3694–3704, <https://doi.org/10.1039/c7ra10688b>.
- [62] S. Deng, L. Cao, Z. Lin, W. Qiu, K. Liang, W. Li, Nanodiamond as an efficient nucleating agent for polyphenylene sulfide, *Thermochim. Acta* 584 (2014) 51–57, <https://doi.org/10.1016/j.tca.2014.03.017>.
- [63] S. Morimune-Moriya, S. Yada, N. Kuroki, S. Ito, T. Hashimoto, T. Nishino, Strong reinforcement effects of nanodiamond on mechanical and thermal properties of polyamide 66, *Compos. Sci. Technol.* 199 (2020), 108356, <https://doi.org/10.1016/j.compscitech.2020.108356>.
- [64] S. Morimune, M. Kotera, T. Nishino, K. Goto, K. Hata, Poly(vinyl alcohol) nanocomposites with nanodiamond, *Macromolecules* 44 (2011) 4415–4421, <https://doi.org/10.1021/ma200176r>.
- [65] S.V. Panin, D.A. Nguyen, D.G. Buslovich, V.O. Alexenko, A.V. Pervikov, L. A. Kornienko, F. Berto, Effect of various type of nanoparticles on mechanical and tribological properties of wear-resistant peek + ptfe-based composites, *Materials* 14 (2021) 1–23, <https://doi.org/10.3390/ma14051113>.
- [66] A. Augustine, R. Augustine, A. Hasan, V. Raghuvveeran, D. Rouxel, N. Kalarikkal, S. Thomas, Development of titanium dioxide nanowire incorporated poly(vinylidene fluoride-trifluoroethylene) scaffolds for bone tissue engineering applications, *J. Mater. Sci. Mater. Med.* 30 (2019), <https://doi.org/10.1007/s10856-019-6300-4>.
- [67] Q. Zhang, V.N. Mochalin, I. Neitzel, I.Y. Knoke, J. Han, C.A. Klug, J.G. Zhou, P. I. Lelkes, Y. Gogotsi, Fluorescent PLLA-nanodiamond composites for bone tissue engineering, *Biomaterials* 32 (2011) 87–94, <https://doi.org/10.1016/j.biomaterials.2010.08.090>.
- [68] R. Augustine, H.N. Malik, D.K. Singhal, A. Mukherjee, D. Malakar, N. Kalarikkal, S. Thomas, Electrospun polycaprolactone/ZnO nanocomposite membranes as biomaterials with antibacterial and cell adhesion properties, *J. Polym. Res.* 21 (2014), <https://doi.org/10.1007/s10965-013-0347-6>.
- [69] A. Brož, L. Bačáková, P. Stenclová, A. Kromka, Š. Potocký, Uptake and intracellular accumulation of diamond nanoparticles - a metabolic and cytotoxic study, *Beilstein J. Nanotechnol.* 8 (2017) 1649–1657, <https://doi.org/10.3762/BJNANO.8.165>.
- [70] M. Grodzik, J. Szczepaniak, B. Strojny-Cieslak, A. Hotowy, M. Wierzbicki, S. Jaworski, M. Kutwin, E. Soltan, T. Mandat, A. Lewicka, A. Chwalibog, Diamond nanoparticles downregulate expression of CycD and CycE in glioma cells, *Molecules* 24 (2019), <https://doi.org/10.3390/molecules24081549>.
- [71] J. Liao, Y. Yao, C.H. Lee, Y. Wu, P. Li, In vivo biodistribution, clearance, and biocompatibility of multiple carbon dots containing nanoparticles for biomedical application, *Pharmaceutics* 13 (2021), <https://doi.org/10.3390/pharmaceutics13111872>.